Available online at www.sciencedirect.com

ScienceDirect

Ceramics International 40 (2014) 323–329

CERAMICS INTERNATIONAL

www.elsevier.com/locate/ceramint

RHEED and XPS study of cerium interaction with SnO_2 (110) surface

J. Beran[a,b,*], S. Hishita[b], K. Mašek[a], V. Matolín[a], H. Haneda[b]

[a]Charles University, Faculty of Mathematics and Physics, Department of Surface and Plasma Sciences, V Holešovičkách 2, 180 00 Prague 8, Czech Republic
[b]Optical and Electronic Materials Unit, National Institute for Materials Science, 1-1 Namiki, Tsukuba, Ibaraki 305-0044, Japan

Received 1 June 2013; accepted 4 June 2013
Available online 13 June 2013

Abstract

Interaction of cerium with thin epitaxial film of tin dioxide with (110) surface orientation was investigated by methods of X-ray Photoelectron Spectroscopy (XPS) and Reflection High Energy Electron Diffraction (RHEED). Strong interaction of cerium and tin leads to cerium diffusion into the tin dioxide bulk and formation of tin–cerium mixed oxide indicated by highly non-stoichiometric cerium oxide Ce 3d core level spectrum. This process is more pronounced with higher temperature during the deposition of cerium. With higher amount of deposited cerium, the tin dioxide substrate is gradually saturated with cerium atoms and the cerium atoms start to create 3D epitaxial clusters of cerium oxide with the (100) and (111) crystallographic planes parallel to the surface. The clusters show a higher oxidation state than the cerium atoms located in the tin oxide bulk. Oxygen required for the creation of these clusters comes from the tin dioxide substrate, which is partially reduced to metallic tin in this process. At the end of the experiment, we obtained a multilayer system consisting of layers of partially reduced tin dioxide, tin–cerium mixed oxide and top layer of partially reduced epitaxial grains of cerium oxide.

Keywords: A. Grain growth; B. Spectroscopy; D. CeO_2

1. Introduction

Cerium oxide, or ceria, has attracted a lot of interest in recent years due to its importance for a variety of modern technologies like electronic and optical applications. Cerium oxide also serves as an important element of commercial catalysts. Typical reaction using cerium oxide is for example the oxidation of CO over cerium oxide supported platinum [1]. This property of cerium oxide is used for example in automotive industry for processing of waste gases in combustion engines. Cerium oxide is also a promising material for use as a cathode material in solid oxide fuel cells. Tin dioxide, on the other hand, is widely used in gas sensing applications, for example in carbon monoxide sensors [2]. Also, being a semiconducting wide-bandgap oxide that is transparent for visible light and has a relatively high electrical conductivity, tin dioxide finds a lot of possible uses in various electronic devices [3].

Cerium oxide is known to exist in two distinct chemical configurations—CeO_2 having fluorite structure and Ce_2O_3 having either cubic or hexagonal structure [4]. Only CeO_2 is stable under atmospheric conditions [5]. While the cerium oxide single crystals are not readily available due to various reasons, great advances have been recently made in preparation of thin epitaxial films of cerium oxide on a number of substrates like Pt [6], Cu [7], Al_2O_3 [8] and $SrTiO_3$ [9]. These epitaxial films are particularly suitable for model studies of cerium oxide catalytic properties and its interactions with other elements due to simplified conditions of the surveyed process.

Catalytic properties of cerium oxide originate from its easy stoichiometric alteration from Ce^{4+} to Ce^{3+} which is accompanied by a release of oxygen into the surrounding atmosphere and creation of oxygen vacancies on the oxide surface, which then act as catalytically active sites. This transformation has relatively low activation energy and can be reversed by simple annealing in oxygen [10]. In this way, the cerium oxide acts as

*Corresponding author. Tel.: +420 221 912 313.
E-mail address: jan.beran@outlook.cz (J. Beran).

0272-8842/$ - see front matter © 2013 Elsevier Ltd and Techna Group S.r.l. All rights reserved.
http://dx.doi.org/10.1016/j.ceramint.2013.06.005

an oxygen reservoir regulating the partial pressure of oxygen over its surface. This property of cerium oxide is known as the Oxygen Storage Capacity and can be improved by suitable metal or metal-oxide additives which interact strongly with cerium and cause its partial reduction.

Photoelectron spectroscopy of the Ce 3d level is a suitable tool for study of cerium oxide reduction and the transition from Ce^{4+} to Ce^{3+}. The electronic structure of cerium oxide is characterized by empty 4f states for the Ce^{4+} and $4f^1$ configuration of Ce^{3+} [11]. During photoemission these states can recombine with electrons from the valence band and give raise to several configurations in the photoemission final state. These are observed as total of five spin orbit split doubles in the Ce 3d core level spectrum. Three of these doublets belong to Ce^{4+} while two belong to cerium in the Ce^{3+} state [12]. While these spectra are rather difficult to decompose, the ratio of intensities of peaks belonging to the respective oxidation states corresponds closely to the overall oxidation state of the sample.

In the previous works, the interaction of tin atoms with the atomically flat surfaces of cerium oxide was investigated [13,14] and the creation of tin–cerium mixed oxide was described [12,15]. This mixed oxide is known to exhibit higher catalytic activity then the individual pure oxides [16]. The strong interaction between the two elements leads to tin diffusion into the sample, where the mixed oxide is created [15]. In order to get better understandings of the fundamental processes leading to the creation of the mixed oxide and its catalytic activity, we have investigated a reverse process in this paper—the interaction of cerium atoms with atomically flat single crystal surface of tin dioxide. To our best knowledge, such model system has never been investigated before. This system was investigated by Reflection High-Energy Electron Diffraction (RHEED) and X-ray Photoelectron Spectroscopy (XPS). Combination of these methods allowed us to describe the structural changes of the sample depending on its chemical composition and state.

2. Experimental

All experiments were done in an Ultra High Vacuum (UHV) chamber with base pressure below 3×10^{-8} Pa. As a substrate for the experiment, we used commercially available TiO_2 single crystals (10 mm × 10 mm × 0.5 mm) with atomically flat (110) surface. The crystals were cleaned in situ by cycles of Ar^+ ion sputtering (5000 eV, 15 μA/cm^2) and annealing at 1000 °C in vacuum, until no impurities were detectable by XPS and a sharp diffraction pattern was obtained by LEED and RHEED. Sample was then reoxidized by annealing at 1000 °C in an oxygen flow.

Tin dioxide epitaxial films with the (110) surface orientation were prepared by reactive evaporation of metallic tin in oxygen atmosphere at the substrate temperature of 500 °C. Tin was evaporated from Knudsen effusion cell at 910 °C. As an oxygen source, we used 5×10^{-3} Pa of NO_2 gas pyrolyzed by hot filament at 800 °C. The SnO_2 film and its preparation are described in more detail in [17].

Cerium was deposited in UHV from Knudsen effusion cell at the temperature of 1300 °C. Under these conditions, cerium was not oxidized when deposited on metallic substrate. The deposition rate was calculated from intensity decrease of the Ti 2p core level photoelectron spectrum. Assuming the mean free path of signal electrons in CeO_2 is 1.8 nm, as calculated by the TPP2 formula [18], the deposition rate was estimated as 0.03 nm/min.

RHEED diffraction patterns were taken using primary electron energy of 15 keV and pictures were taken by a CCD camera. The sample lattice parameters were calculated from the distances of diffraction features, which were determined by the method of sub-pixel detection with precision better than 0.5% [19]. All XPS spectra were taken at $h\upsilon = 1486.6$ eV (Al K_α) and measured at the normal and 60° emission angle by Escalab 200-X electron analyzer supplied by VG Scientific.

3. Results and discussion

The tin dioxide film with 3 nm thickness was prepared by previously described procedure and gave a sharp RHEED diffraction pattern consisting of rods corresponding to a flat surface of epitaxial tin dioxide with the cassiterite structure and (110) surface orientation. Measurement of diffraction spot distances gave the value of lattice parameter of $a = 0.477$ nm and $c = 0.321$ nm. Both these values were less than 1% different from the bulk values of tin dioxide [20]. The Sn $3d_{5/2}$ and O 1 s XPS spectra taken from the SnO_2 substrate are presented in Figs. 1 and 2, respectively. The Sn $3d_{5/2}$ peak is located at the binding energy of 486.4 eV, while the O 1 s peak is located at the binding energy of 530.1 eV. Both these values correspond to stoichiometric tin dioxide [21,22].

Metallic cerium was deposited onto this substrate at RT (Room Temperature) and 300 °C respectively. In both cases, we deposited up to 1 nm of cerium in four deposition steps. XPS spectra and RHEED images were recorded after each step. The Ce 3d spectra taken after the first deposition step of 0.25 nm of Ce at the 60° emission angle decomposed into five doublets representing Ce^{3+} and Ce^{4+} oxidation states are presented in Fig. 3a and b. In both cases, these spectra correspond to a non-stoichiometric and highly reduced cerium oxide which is evidenced by very low intensity of the $3d_{3/2}$ peak located at the binding energy of 917 eV. The Ce^{3+}/Ce^{4+} intensity ratio of peaks belonging to Ce^{3+} ($3d_{5/2}$ peak binding energies 880.5 eV and 885.7 eV) and Ce^{4+} ($3d_{5/2}$ peaks binding energies 882.6 eV, 888.5 eV and 898.6 eV) was used to express the overall oxidation state of the cerium oxide. We obtained $Ce^{3+}/Ce^{4+} = 2.30$ for deposition at RT and $Ce^{3+}/Ce^{4+} = 1.79$ for deposition at 300 °C. The spectra were also measured at the normal emission angle. In this case the peak intensity ratios were lower giving values of 2.03 for deposition at RT and 1.68 for deposition at 300 °C, which means that the overall oxidation state of the cerium oxide was higher. The difference in the oxidation states is discussed later in the text. It can be concluded that the cerium oxide oxidation state is almost homogenous throughout the sample and

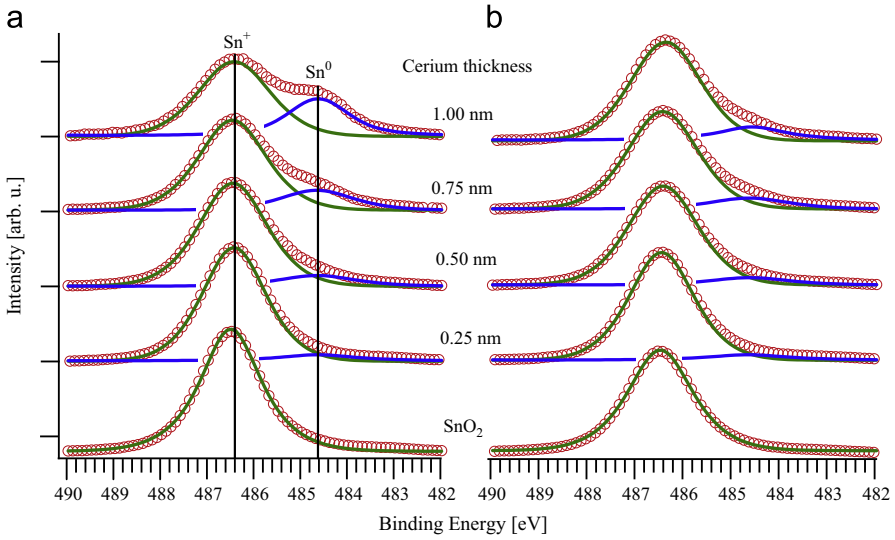

Fig. 1. Sn $3d_{5/2}$ XPS spectra taken during the experiment after the depositions at RT (a) and 300 °C (b) with different thickness of deposited cerium. Spectra were taken at 60° emission angle and normalized for better readability.

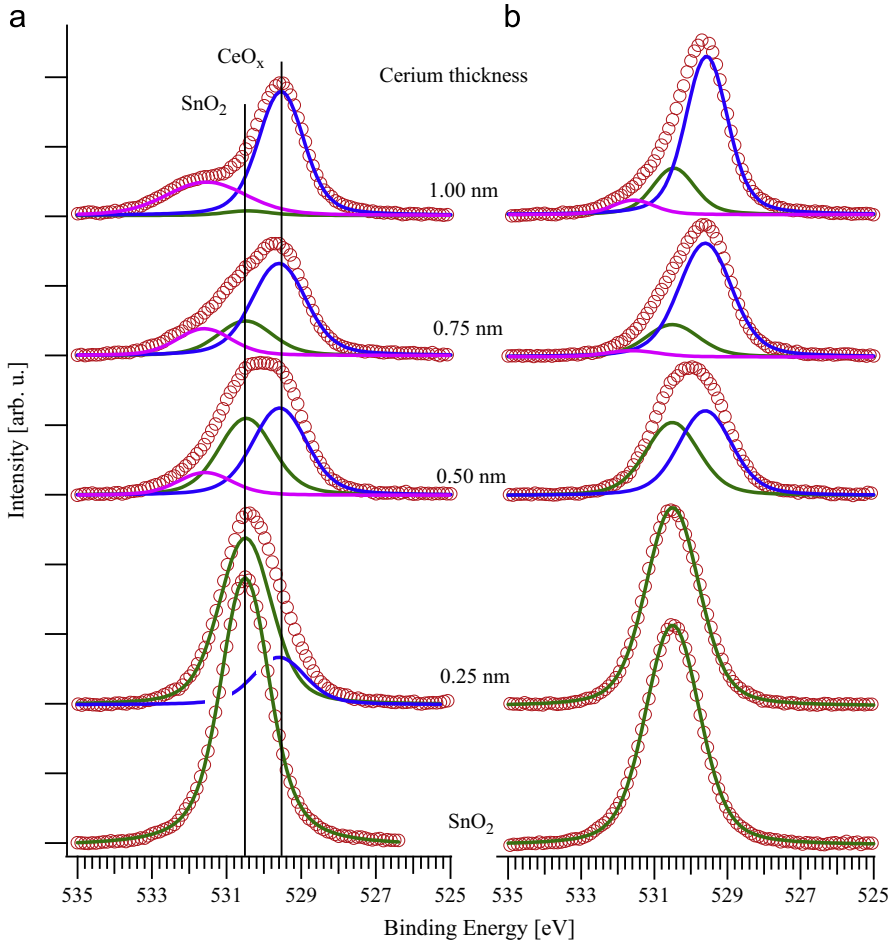

Fig. 2. O 1s XPS spectra taken during the experiment after the depositions at RT (a) and 300 °C (b) with different thickness of deposited cerium. Spectra were taken at 60° emission angle.

up to the information depth of the XPS method. The more reduced cerium oxide was found at the surface.

The Sn 3d spectra taken after the first depositions of cerium are presented in Fig. 1. There are two effects to be observed. First, a new chemical state of tin has appeared at the lower binding energy side of the spectrum at binding energy of 484.6 eV. This can be attributed to metallic tin [23]. Second, the Full Width at Half Maximum (FWHM) of the SnO_2 peak

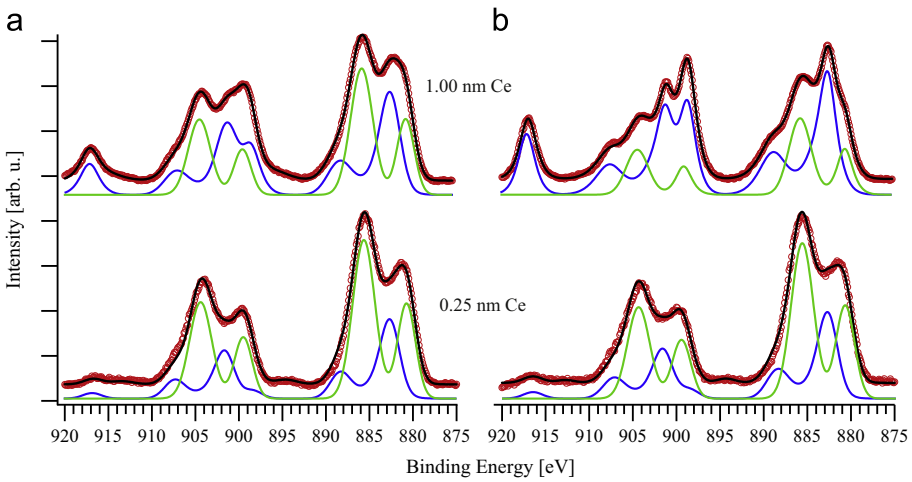

Fig. 3. XPS spectra of the Ce 3d core level taken after depositions at RT (a) and 300 °C (b) at the 60° emission angle. The spectra were fitted with five doublets consistent with the Ce 3d level electronic structure and normalized to have the same overall intensity, to highlight the differences in their composition. Doublets belonging to individual oxidation states were merged together–blue line belongs to Ce^{4+}, light green line belongs to Ce^{3+}. (For interpretation of the references to color in this figure legend, the reader is referred to the web version of this article).

has increased from 1.58 eV of the pure SnO_2 to 1.72 eV. This might be evidence of evolution of a new chemical state, which is located very close to the SnO_2 peak. A new peak has also appeared in the O 1s spectrum at the binding energy of 529.6 eV (see Fig. 2), which can be attributed to oxygen atoms bound in the cerium oxide [24].

The RHEED diffraction patterns taken after the first deposition of cerium (not shown here) are composed of a very weak set of wide diffraction rods and diffuse background of higher intensity. It is unclear, if these rods belong to the tin dioxide substrate or to the cerium oxide deposit. In fact, these lines are placed in between the expected positions of SnO_2 and CeO_2 lines. It is therefore possible, that the observed weak lines are a combination of both diffraction features. The elevated intensity of diffuse background is consistent with loss of the surface crystal arrangement caused by cerium diffusion into the tin oxide lattice.

From the data presented above, we assume that the diffusion of a significant amount of cerium into the SnO_2 substrate and a strong metal substrate interaction led to the formation of tin–cerium mixed oxide. This claim is supported by the low oxidation state of the cerium and the appearance of a new oxidation state in the Sn 3d spectrum at binding energy being very close to binding energy of the Sn $3d_{5/2}$ peak obtained for pure tin dioxide. The difference between the overall cerium oxidation states, expressed by the Ce^{3+}/Ce^{4+} ratio, at different deposition temperatures is given by a higher diffusion rate of Ce at the temperature of 300 °C. This also enables greater mobility of oxygen atoms in the tin dioxide substrate and therefore easier oxidation of cerium.

In the next stages of the experiment, we gradually deposited more cerium on the tin dioxide substrate up to 1 nm of thickness. The RHEED diffraction patterns taken during the experiment showed an appearance of diffraction spots that originated from transmission diffraction on 3D epitaxial clusters. These spots became sharper and more intense with increasing cerium loading. An example of the diffraction patterns taken after deposition at 300 °C, along with their respective interpretations, is given in Fig. 4. The patterns taken after deposition at RT were qualitatively identical, but exhibited higher background intensity. This is probably due to lower crystallographic arrangement of the epitaxial clusters at lower temperatures. The patterns in Fig. 4 were taken in the [110], [112] and [001] directions of the substrate. Due to almost square symmetry of the SnO_2 (110) plane, the angle between these directions is 46.4° and 43.6°, respectively. The spots in Fig. 4a and b originate from the (110) and (100) reciprocal planes of cerium oxide with the [001] direction perpendicular to the surface. Since the angle between these two patterns is almost 45°, they can be attributed to epitaxial clusters of cerium oxide with the (100) crystallographic plane parallel to the surface.

The patterns in Fig. 4a and c also include another set of spots that cannot be explained by this interpretation. These extra spots originate from (112) and (111) reciprocal planes of cerium oxide with the [111] direction perpendicular to the surface and can be attributed to clusters with (111) epitaxial plane parallel to the substrate. The pattern in Fig. 4c consists of two lattices, that are mirrored along the [111] direction with respect one to each other. This means that the population of epitaxial clusters has two orientations given by different ABCABC stacking of the (111) planes in the FCC structure. This effect is called double positioning and cannot be observed in Fig. 4a due to the symmetry of (112) reciprocal plane of cerium oxide along the [111] direction.

These two populations of cerium oxide epitaxial clusters can also be described by the following epitaxial relations and are shown in schematic drawing in Fig. 5.

$$\begin{matrix} CeO_2\ (100) \| SnO_2\ (110) \\ CeO_2\ [110] \| SnO_2\ [001] \end{matrix} \qquad \begin{matrix} CeO_2\ (111) \| SnO_2\ (110) \\ CeO_2\ [110] \| SnO_2\ [001] \end{matrix}$$

The lattice mismatch of the tin dioxide and the cerium oxide clusters can be expressed by accommodation parameters that

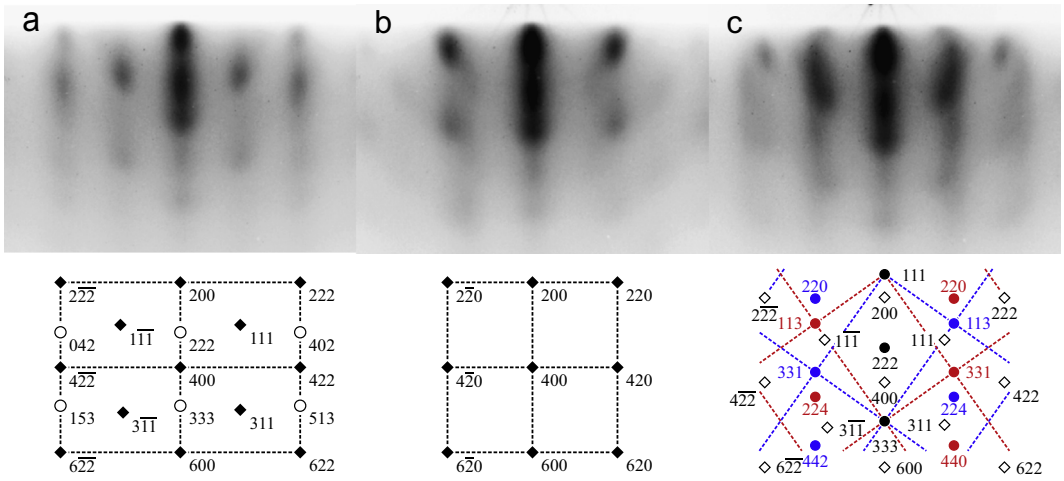

Fig. 4. RHEED diffraction patterns of cerium oxide clusters taken after the deposition of 1 nm of cerium at the temperature of 300 °C and their respective interpretations. The patterns were taken in the [110] (a), [112] (b) and [001] (c) directions of the substrate surface. The full squares in (a) and (b) represent the (110) and (100) reciprocal planes of cerium oxide, while the open circles in (a) represent the (112) reciprocal plane of cerium oxide with the [111] direction perpendicular to the surface. Full circles in (c) represent the two (111) planes with [111] direction perpendicular to the surface, while the open squares represent the (110) plane.

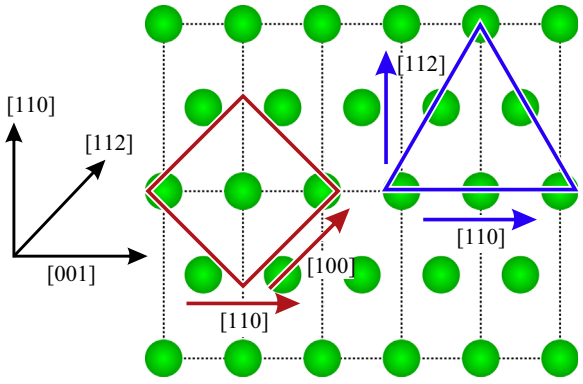

Fig. 5. Schematic drawing of the cerium oxide clusters epitaxy on the surface of SnO_2 (111). The red square and blue triangle represent the two populations of (100) and (111) cerium oxide grains, respectively. (For interpretation of the references to color in this figure legend, the reader is referred to the web version of this article.)

are calculated as a ratio of inter-reticular distances of the substrate and deposit along a given crystallographic direction. The parameters calculated for both populations along the [110], [001] and [112] directions are presented in Table 1. The epitaxial growth of cerium oxide clusters seems to be achieved by matching symmetry of the substrate and deposit lattices for the (100) population, while in the (111) population epitaxy is driven by good crystallographic arrangement of the clusters with respect to the substrate.

In the XPS spectra of the Ce 3d core level, we observed that with the higher amount of deposited cerium, the overall oxidation state of the CeO_x layer was getting closer to the stoichiometric CeO_2. Due to very low oxygen partial pressure in the residual atmosphere in the experimental chamber, oxidation of cerium proceeds by taking the oxygen atoms from the tin dioxide substrate. The evolution of the Ce^{3+}/Ce^{4+} peak intensity ratio calculated from Ce 3d core level spectra taken

Table 1
Accommodation parameters of both cerium oxide clusters populations in the three main crystallographic directions of the tin dioxide substrate.

Epitaxy	[110]	[001]	[112]
(100)	0.57	1.2	0.58
(111)	0.99	1.2	–

during the experiment is plotted in Fig. 6. We can see that the cerium oxide layer is showing some limit value of oxidation, which is dependent on the temperature during the deposition. These values are 1.2 for deposition at RT and 0.5 for deposition at 300 °C at 1 nm of deposited cerium. The respective Ce 3d spectra are shown in Fig. 3. We can also see, that the layer deposited at RT reaches this limit value earlier than the one deposited at 300 °C. This phenomenon can be explained by the fact, that at higher temperature during the deposition, the cerium atoms can diffuse deeper into the substrate and therefore, the saturation of tin dioxide with cerium atoms will be reached only at higher deposited amount. After the saturation is reached, excessive cerium atoms remain on the surface and form epitaxial clusters of cerium oxide. Again, the higher temperature allows for greater mobility of oxygen atoms in the substrate, which probably accounts for the higher overall oxidation state of the clusters deposited at 300 °C. This can be also the reason why this layer has higher homogeneity during the whole experiment, as seen from the very small difference between the Ce^{3+}/Ce^{4+} peak intensity ratios calculated from the Ce 3d spectra taken at 60° and normal emission, compared to those taken after depositions at RT.

The spectra of Sn $3d_{5/2}$ taken during the experiment (see Fig. 1) show that the peak of metallic tin was slowly growing in intensity with increased cerium loading. This effect was more pronounced during the deposition at RT. Again, this may be caused by differences between oxygen atom diffusion

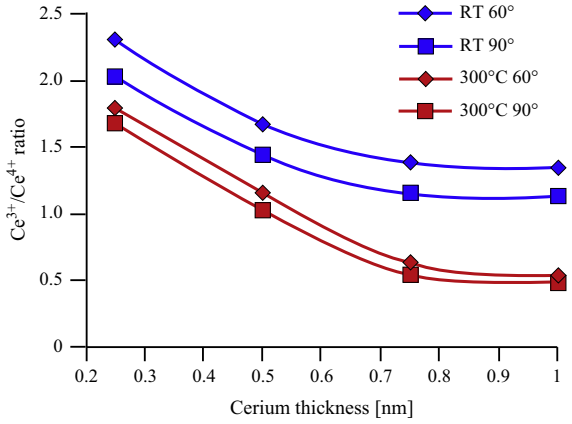

Fig. 6. The evolution of the Ce^{3+}/Ce^{4+} peak intensity ration calculated from the Ce 3d during the experiment. The spectra were measured for depositions at RT and 300 °C and at 60°and normal emission angles.

coefficients. At lower temperature, surface layer of cerium is oxidized by oxygen atoms taken from the tin dioxide substrate, while at higher temperatures it allows for diffusion of oxygen atoms even from the titanium dioxide substrate. The O 1s spectra in Fig. 2 show an increasing intensity of peak belonging to the oxygen bound to cerium oxide and decreasing intensity of the tin dioxide peak as can be expected from increased amount of deposited cerium. Moreover, a new weak peak appeared at the binding energy of 531.5 eV. The intensity of this peak was much larger for measurements taken after the RT depositions and the peak disappeared after annealing at 300 °C. Accordingly to these results we attributed this peak to adsorbed water and CO species in agreement with literature [25].

4. Conclusion

In this paper, we investigated the interaction of a flat single crystal tin dioxide (110) surface with metallic cerium deposited at various temperatures. We deduced that cerium atoms diffused into the substrate creating a tin–cerium mixed oxide. From the Ce 3d spectra measured during the experiment we found that the overall oxidation state of cerium oxide increased with increasing deposition temperature and amount of deposited cerium, owing to easier diffusion of the oxygen atoms through the tin–cerium mixed oxide. The RHEED measurements showed that after the layer saturation by cerium, excess of cerium atoms remained on the surface, where they created epitaxial cerium oxide islands with (100) and (111) surface orientations. At the end of the experiment, we obtained a complex system consisting of layers of partially reduced tin oxide, tin–cerium mixed oxide and top layer of partially reduced cerium oxide epitaxial clusters. This could be a promising system for future investigation of high activity cerium oxide based catalyst.

Acknowledgments

This work was supported by the projects LD11047 and LD13054 financed by the Ministry of Education of the Czech Republic and 204/11/1183 financed by Grant Agency of Czech Republic. Author also acknowledges the Joint Graduate School Fellowship from the National Institute for Materials Science.

References

[1] G.N. Vayssilov, Y. Lykhach, A. Migani, T. Staudt, G.P. Petrova, N. Tsud, T. Skála, A. Bruix, F. Illas, K.C. Prince, V. Matolín, K.M. Neyman, J. Libuda, Support nanostructure boosts oxygen transfer to catalytically active platinum nanoparticles, Nature Materials 10 (4) (2011) 310–315.
[2] O.V. Anisimov, V.I. Gaman, N.K. Maksimova, S.M. Mazalov, E.V. Chernikov, Electrical and gas-sensitive properties of a resistive thin-film sensor based on tin dioxide, Semiconductors 40 (6) (2006) 704–709.
[3] H. Kim, A. Pique, J.S. Horwitz, H. Mattoussi, H. Murata, Z.H. Kafafi, D. B. Chrisey, Indium tin oxide thin films for organic light-emitting devices, Applied Physical Letters 74 (23) (1999) 3444–3446.
[4] G. Adachi, N. Imanaka, The binary rare earth oxides, Chemical Reviews 98 (4) (1998) 1479–1514.
[5] J.L.F. Da Silva, Stability of the Ce_2O_3 phases: a DFT+U investigation, Physical Review B 76 (19) (2007) 193108.
[6] K.D. Schierbaum, Ordered ultra-thin cerium oxide overlayers on Pt(111) single crystal surfaces studied by LEED and XPS, Surface Science 399 (1) (1998) 29–38.
[7] K. Mašek, J. Beran, V. Matolín, RHEED study of the growth of cerium oxide on Cu(111), Applied Surface Science 259 (2012) 34–38.
[8] G. Linker, R. Smithey, J. Geerk, F. Ratzel, R. Schneider, A. Zaitsev, The growth of ultra-thin epitaxial CeO_2 films on r-plane sapphire, Thin Solid Films 471 (1–2) (2005) 320–327.
[9] Y.J. Kim, Y. Gao, G.S. Herman, S. Thevuthasan, W. Jiang, D.E. McCready, S.A. Chambers, Growth and structure of epitaxial CeO_2 by oxygen-plasma-assisted molecular beam epitaxy, Journal of Vacuum Science Technology A 17 (3) (1999) 926–935.
[10] W.D. Xiao, Q.L. Guo, E.G. Wang, Transformation of CeO_2(111) to Ce_2O_3(0001) films, Chemical Physics Letters 368 (5–6) (2003) 527–531.
[11] S. Fabris, G. Vicario, G. Balducci, S. de Gironcoli, S. Baroni, Electronic and atomistic structures of clean and reduced ceria surfaces, Journal of Physical Chemistry B 109 (48) (2005) 22860–22867.
[12] T. Skála, F. Šutara, K.C. Prince, V. Matolín, Cerium oxide stoichiometry alteration via Sn deposition: influence of temperature, Journal of Electron Spectroscopy 169 (1) (2009) 20–25.
[13] V. Matolín, M. Cabala, V. Cháb, I. Matolínová, K.C. Prince, M. Škoda, F. Šutara, T. Skála, K. Veltruská, A resonant photoelectron spectroscopy study of Sn(O_x) doped CeO_2 catalysts, Surface and Interface Analysis 40 (3–4) (2008) 225–230.
[14] K. Mašek, M. Václavů, P. Bábor, V. Matolín, Sn–CeO_2 thin films prepared by RF magnetron sputtering: XPS and SIMS study, Applied Surface Science 255 (13-14) (2009) 6656–6660.
[15] M. Škoda, M. Cabala, V. Cháb, K.C. Prince, L. Sedláček, T. Skála, F. Šutara, V. Matolín, Sn interaction with the CeO_2(111) system: bimetallic bonding and ceria reduction, Applied Surface Science 254 (14) (2008) 4375–4379.
[16] T.B. Nguyen, J.P. Deloume, V. Perrichon, Study of the redox behaviour of high surface area CeO_2–SnO_2 solid solutions, Applied Catalysis A: General 249 (2) (2003) 273–284.
[17] S. Hishita, P. Janeček, H. Haneda, Epitaxial growth of tin oxide film on TiO_2(110) using molecular beam epitaxy, Journal of Crystal Growth 312 (20) (2010) 3046–3049.
[18] S. Tanuma, C.J. Powell, D.R. Penn, Calculations of electron inelastic mean free paths. V. Data for 14 organic-compounds over the 50–2000 EV range, Surface and Interface Analysis 21 (3) (1994) 165–176.
[19] V. Matolín, B. Peuchot, Subpixel detection in video rheed image-analysis, Thin Solid Films 259 (1) (1995) 65–69.
[20] W.H. Baur, A.A. Khan, Rutile-type compounds.4. SiO_2, GeO_2 and a comparison with other rutile-type structures, Acta Crystall B-Stru B 27 (15) (1971) 2133.

[21] G.T. Baronetti, S.R. Demiguel, O.A. Scelza, A.A. Castro, state of metallic phase in Pt-Sn/Al_2O_3 catalysts prepared by different deposition techniques, Applied Catalysis 24 (1–2) (1986) 109–116.
[22] A.W.C. Lin, N.R. Armstrong, T. Kuwana, X-Ray photoelectron auger electron spectroscopic studies of tin and indium metal foils and oxides, Analytical Chemistry 49 (8) (1977) 1228–1235.
[23] R.I. Hegde, S.R. Sainkar, S. Badrinarayanan, A.P.B. Sinha, A Study of dilute tin alloys by X-ray photoelectron-Spectroscopy, Journal of Electron Spectroscopy 24 (1) (1981) 19–25.
[24] A. Dauscher, L. Hilaire, F. Lenormand, W. Muller, G. Maire, A. Vasquez, Characterization by XPS and XAS of supported Pt/TiO_2–CeO_2 catalysts, Surface and Interface Analysis 16 (1–12) (1990) 341–346.
[25] M.A. Henderson, C.L. Perkins, M.H. Engelhard, S. Thevuthasan, C.H.F. Peden, Redox properties of water on the oxidized and reduced surfaces of CeO_2(111), Surface Science 526 (1-2) (2003) 1–18.